JACS
JOURNAL OF THE AMERICAN CHEMICAL SOCIETY

ARTICLE

pubs.acs.org/JACS

Stoichiometric and Oxygen-Rich $M_2O_n^-$ and M_2O_n (M = Nb, Ta; n = 5−7) Clusters: Molecular Models for Oxygen Radicals, Diradicals, and Superoxides

Hua-Jin Zhai,[†] Xian-Hui Zhang,[‡,§] Wen-Jie Chen,[‡,§] Xin Huang,[‡,§,*] and Lai-Sheng Wang[†,*]

[†]Department of Chemistry, Brown University, Providence, Rhode Island 02912, United States

[‡]Department of Chemistry, Fuzhou University, Fuzhou, Fujian 350108, P. R. China

[§]State Key Laboratory of Structural Chemistry, Fuzhou, Fujian 350002, P. R. China

Supporting Information

ABSTRACT: We investigated the structures and bonding of two series of early transition-metal oxide clusters, $M_2O_n^-$ and M_2O_n (M = Nb, Ta; n = 5−7) using photoelectron spectroscopy (PES) and density-functional theory (DFT). The stoichiometric M_2O_5 clusters are found to be closed shell with large HOMO−LUMO gaps, and their electron affinities (EAs) are measured to be 3.33 and 3.71 eV for M = Nb and Ta, respectively; whereas EAs for the oxygen-rich clusters are found to be much higher: 5.35, 5.25, 5.28, and 5.15 eV for Nb_2O_6, Nb_2O_7, Ta_2O_6, and Ta_2O_7, respectively. Structural searches at the B3LYP level yield triplet and doublet ground states for the oxygen-rich neutral and anionic clusters, respectively. Spin density analyses reveal oxygen radical, diradical, and superoxide characters in the oxygen-rich clusters. The $M_2O_7^-$ and M_2O_7 clusters, which can be viewed to be formed by $M_2O_5^{-/0} + O_2$, are utilized as molecular models to understand dioxygen activation on $M_2O_5^-$ and M_2O_5 clusters. The O_2 adsorption energies on the stoichiometric M_2O_5 neutrals are shown to be surprisingly high (1.3−1.9 eV), suggesting strong capabilities to activate O_2 by structural defects in Nb and Ta oxides. The PES data also provides valuable benchmarks for various density functionals (B3LYP, BP86, and PW91) for the Nb and Ta oxides.

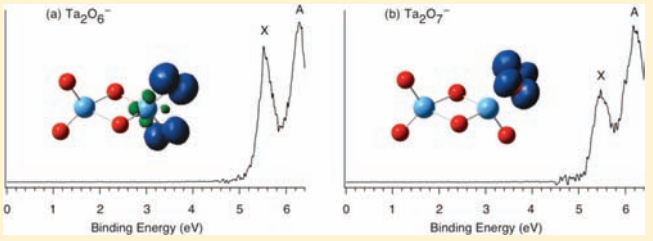

1. INTRODUCTION

Structural and electronic defects are common on surfaces of transition-metal oxides, which are responsible for the interesting chemical, optical, magnetic, and catalytic properties of this class of technologically important materials.[1,2] Adsorption and activation of dioxygen on metal centers are the initial steps of oxidation reactions on oxide surfaces, resulting in catalytically active oxygen radicals or superoxides.[3] Among the catalytic applications of group VB oxides,[4−9] the Nb oxides catalyze numerous reactions and can serve as effective catalytic supports as well.[5,6] Both Nb and Ta oxides are also efficient catalytic promoters[5−8] and have been considered for photocatalysts.[9] Chemical processes taking place in real oxide catalysts are extremely complicated. Thus, our current understanding of the nature of active oxygen species on Nb and Ta oxides and of the interactions of oxygen with Nb and Ta centers is rather limited at the molecular level.[5−9]

In the past decade, increasing research efforts have been directed to gas-phase transition-metal oxide clusters,[10−30] which can provide well-defined molecular models toward mechanistic insights into the complex surface processes and catalysis.[31] There have been numerous gas-phase studies on Nb and Ta oxide clusters.[10,15−20,27,30,32−35] Chemical reactions of charged Nb (Ta) oxide clusters with hydrocarbon molecules were reported.[16,17] Single-photon VUV ionization on neutral M_mO_n (M = V, Nb, Ta) clusters showed that M_2O_5, M_3O_7, and M_4O_{10} clusters are most abundant.[20] Photodissociation of cationic $M_mO_n^+$ (M = V, Nb, Ta) clusters revealed enhanced stability for $M_2O_4^+$, $M_3O_7^+$, and $M_4O_9^+$.[19] Infrared multiple photon dissociation (IR-MPI) spectroscopy allowed structural characterizations for a number of positively charged Nb (Ta) oxide clusters, such as $Nb_2O_6^+$, $Nb_3O_8^+$, and $Ta_3O_8^+$.[10,18] We are interested in using anion photoelectron spectroscopy (PES) and computational chemistry to investigate the structures and bonding in early transition-metal oxide clusters and to discover cluster models for catalytic active centers. In a recent study, we investigated the electronic structure of the $Nb_4O_{10}^-$ and $Ta_4O_{10}^-$ tetrahedral cage clusters as well as polyhedral cage clusters $(V_2O_5)_n^-$ (n = 2−4).[27] We also discovered δ aromaticity in the $Ta_3O_3^-$ cluster.[28] However, the electronic structure of Nb and Ta oxide clusters remains poorly understood, and available PES studies are primarily centered on the metal-rich Nb and Ta oxide clusters.[27,28,30,34]

Received: November 9, 2010
Published: February 09, 2011

In the current contribution, we report a combined PES and density-functional theory (DFT) study of stoichiometric and oxygen-rich $M_2O_n^-$ and M_2O_n (M = Nb, Ta; n = 5−7) clusters in the gas phase. Well-defined PES spectra reveal large energy gaps in the $Nb_2O_5^-$ and $Ta_2O_5^-$ clusters and very high electron binding energies for the O-rich clusters, $Nb_2O_n^-$ and $Ta_2O_n^-$ (n = 6, 7). Structural searches at the B3LYP level yield open-shell ground states for all eight O-rich anionic and neutral clusters: triplets for neutrals and doublets for anions. The stoichiometric M_2O_5 neutral clusters and their $M_2O_5^-$ anions adopt singlet and doublet ground states, respectively. Electron spin density analyses show that the two $M_2O_5^-$ anion clusters each possess a localized 4d/5d spin, giving rise to a tricoordinate M^{4+} reduced center. Intriguing oxygen radical, diradical, and superoxide nature is revealed for the eight O-rich clusters, where the M_2O_n (n = 6, 7) neutral clusters appear to be as effective as their $M_2O_n^-$ anions in the stabilization of active oxygen species, and the neutral clusters can further double the number of active oxygen species. The $M_2O_7^-$ and M_2O_7 clusters are used as molecular models to study the dioxygen activation on $M_2O_5^-$ and M_2O_5 clusters, and the O_2 adsorption energies on the stoichiometric M_2O_5 neutrals are found to be remarkably high (1.3−1.9 eV). These observations are in contrast to those observed in O-rich $W_2O_8^-/W_3O_{11}^-$ clusters,[26] suggesting that the Nb and Ta centers are more reactive toward O_2 and can more effectively stabilize the radical, diradical, and superoxide species.

2. EXPERIMENTAL AND COMPUTATIONAL METHODS

2.1. Photoelectron Spectroscopy. The experiments were carried out using a magnetic-bottle PES apparatus equipped with a laser vaporization cluster source, details of which have been described previously.[36] Briefly, the Nb (Ta) oxide clusters were produced by laser vaporization of a pure Nb (Ta) disk target in the presence of a He carrier gas seeded with 0.5% O_2 and analyzed using a time-of-flight mass spectrometer. The $Nb_2O_n^-$ and $Ta_2O_n^-$ (n = 5−7) clusters were each mass selected and decelerated before being photodetached. The photodetachment experiments were conducted at the 193 nm (6.424 eV) photon energy from an ArF excimer laser. Effort was made to choose colder clusters (those with long resident times in the nozzle) for photodetachment, which was shown previously to be critical for obtaining high-quality PES data.[37] Photoelectrons were collected at nearly 100% efficiency by the magnetic bottle and analyzed in a 3.5 m long electron flight tube. The PES spectra were calibrated using the known spectra of Au^-, and the energy resolution of the apparatus was $\Delta E_k/E_k \approx 2.5\%$, that is, ∼25 meV for 1 eV electrons.

2.2. Computational Methods. The DFT calculations were carried out using the hybrid B3LYP functional.[38,39] The calculations are spin restricted for closed-shell molecules and spin unrestricted for open-shell species. The UB3LYP calculations turned out to have little spin contamination. The global minimum searches were performed using analytical gradients with the Stuttgart relativistic small core basis set and efficient core potential[40,41] augmented with two f-type and one g-type polarization functions for Nb [$\zeta(f)$ = 0.261, 0.970; $\zeta(g)$ = 0.536] and Ta [$\zeta(f)$ = 0.210, 0.697; $\zeta(g)$ = 0.472] as recommended by Martin and Sundermann[42] and the aug-cc-pVTZ basis set for oxygen.[43] Scalar relativistic effects, that is, the mass velocity and Darwin effects, were taken into account via the quasi-relativistic pseudopotentials. Vibrational frequency calculations were done to verify the nature of the stationary points. Vertical electron detachment energies (VDEs) were calculated using the generalized Koopmans' theorem by adding a correction term to the eigenvalues of the anion.[44] The correction term was calculated as $\delta E = E_1 - E_2 - \varepsilon_{HOMO}$, where E_1 and E_2 are the total energies of the anion and neutral, respectively, in their ground states at the anion equilibrium geometry and ε_{HOMO} corresponds to the eigenvalue of the highest occupied molecular orbital (HOMO) of the anion. The relative energies of the low-lying structures were further evaluated via single-point calculations at the coupled cluster [CCSD(T)][45] level with the Nb,Ta/Stuttgart+2f1g/O/aug-cc-pVTZ basis sets at the B3LYP geometries. For open-shell systems, the R/UCCSD(T) approach was used, where a restricted open-shell Hartree−Fock (ROHF) calculation was initially performed and the spin constraint was relaxed in the correlation treatment. Additional BP86 and PW91 calculations[46,47] were performed on the ground-state structures for the O-rich anion clusters to test the performance of different DFT functionals. All DFT calculations were performed using the Gaussian 03 package,[48] and the CCSD(T) calculations were done using the MOLPRO 2010.1 package.[49]

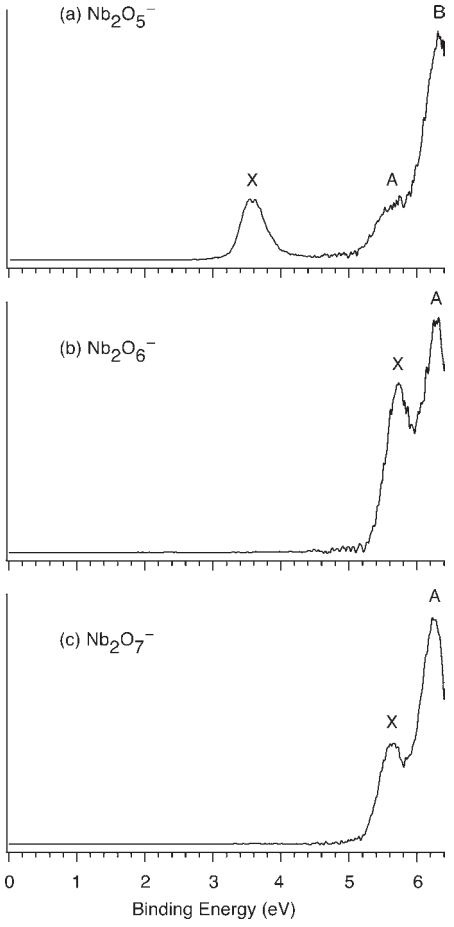

Figure 1. Photoelectron spectra of (a) $Nb_2O_5^-$, (b) $Nb_2O_6^-$, and (c) $Nb_2O_7^-$ at 193 nm.

3. EXPERIMENTAL RESULTS

The 193 nm PES data for $Nb_2O_n^-$ and $Ta_2O_n^-$ (n = 5−7) are shown in Figures 1 and 2, respectively. The observed spectral bands are labeled with letters (X, A, and B), and the measured adiabatic detachment energies (ADEs) and VDEs are summarized in Table 1.

3.1. $Nb_2O_5^-$ and $Ta_2O_5^-$. The 193 nm PES spectrum of $Nb_2O_5^-$ (Figure 1a) exhibits three bands (X, A, and B). The ground-state band X is weak with a relatively low binding energy (VDE = 3.58 eV; Table 1). Since no vibrational structures are resolved for band X, the ground-state ADE is evaluated by

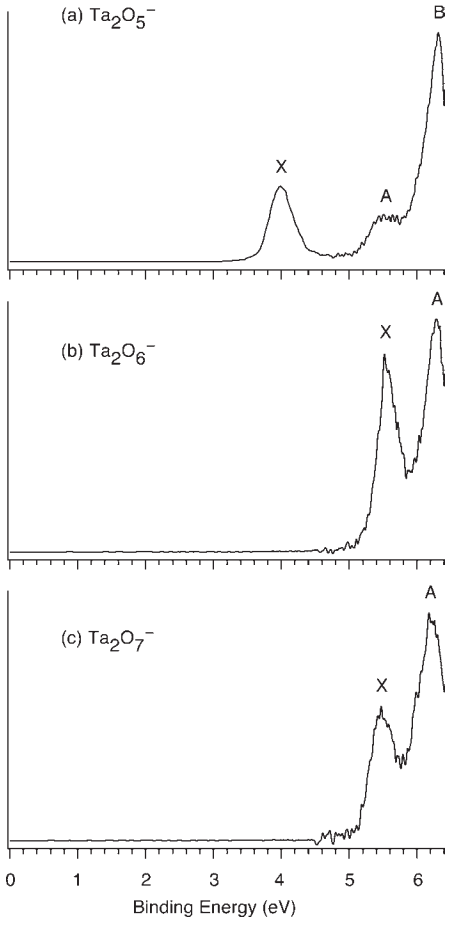

Figure 2. Photoelectron spectra of (a) $Ta_2O_5^-$, (b) $Ta_2O_6^-$, and (c) $Ta_2O_7^-$ at 193 nm.

drawing a straight line along its leading edge and then adding the instrumental resolution to the intersection with the binding energy axis. Although this is an approximate procedure, the well-defined onset of band X allows a fairly accurate ADE value to be obtained: 3.33 ± 0.05 eV, which represents the electron affinity of the Nb_2O_5 neutral cluster. The first excited state, band A, is located at a much higher binding energy (ADE = 5.16 eV; VDE = 5.65 eV), defining a sizable energy gap of 1.83 eV as evaluated from the ADE difference between bands X and A. Band A appears broad and weak. At the highest binding energy, an intense and well-defined band B is observed (VDE = 6.32 eV).

The PES spectrum of $Ta_2O_5^-$ (Figure 2a) is similar to that of $Nb_2O_5^-$, showing two weaker bands, X (ADE = 3.71 ± 0.05 eV; VDE = 3.99 eV) and A (ADE = 5.09 eV; VDE = 5.55 eV), and an intense band B (VDE = 6.31 eV). The X−A energy gap is evaluated to be 1.38 eV for $Ta_2O_5^-$, which is 0.45 eV smaller than that for $Nb_2O_5^-$. The PES spectra suggest that the two stoichiometric clusters, M_2O_5, are closed shell with sizable energy gaps between the HOMO and the lowest unoccupied molecular orbital (LUMO). The extra electron in the $M_2O_5^-$ anions enters the LUMO of the neutral clusters, resulting in the relatively low electron binding energies.

3.2. $Nb_2O_n^-$ and $Ta_2O_n^-$ (n = 6, 7). Qualitatively, the PES spectra for the four O-rich species appear rather similar (Figures 1 and 2): (i) all species show extremely high electron binding energies (>5 eV); (ii) each spectrum displays two well-defined PES bands (labeled as X and A); (iii) all observed PES bands show roughly the same bandwidth (∼0.4−0.5 eV) except that the relative intensity of band A seems to increase from n = 6 to 7. The ground-state VDEs, obtained from the maximum of band X, are 5.74, 5.64, 5.57, and 5.49 eV for $Nb_2O_6^-$, $Nb_2O_7^-$, $Ta_2O_6^-$, and $Ta_2O_7^-$, respectively (Table 1). The ground-state ADEs are obtained from the well-defined onsets of band X as 5.35, 5.25, 5.28, and 5.15 eV, respectively, which also represent the electron affinities of the corresponding neutral clusters. Similarly, the VDEs for band A of the four species are obtained from the maximum of band A. All the obtained ADEs and VDEs are given in Table 1. As will be seen from the DFT calculations below, band A for all four O-rich species (and band B for the stoichiometric species) each contain contributions from multiple electronic transitions. In these cases, the experimental VDEs obtained should be viewed as average values.

4. THEORETICAL RESULTS

The optimized anion and neutral ground-state and low-lying structures (within ∼0.5 eV) at the B3LYP level are presented in Figure 3 for the $M_2O_5^-$ and M_2O_5 clusters and in Figures 4 and 5 for $M_2O_n^-$ and M_2O_n (n = 6, 7), respectively. Alternative optimized geometries are shown in the Supporting Information (Figures S1−S12).

4.1. $Nb_2O_5^-$ and Nb_2O_5. Our extensive structural searches for $Nb_2O_5^-$ (Figure S1) lead to the C_s ($^2A'$) ground state, as shown in Figure 3a. This structure is based on a four-membered Nb_2O_2 ring motif with three additional terminal O atoms, resulting in a tetracoordinated and a tricoordinated Nb. The bridging Nb−O distances are slightly uneven (2.058 versus 1.886 Å). The terminal Nb−O distances are similar (1.74−1.75 Å). Alternative optimized $Nb_2O_5^-$ anion structures, including those with two, one, or three bridging O atoms and in different spin states (Figure S1, Supporting Information), are at least ∼1.2 eV higher in energy, suggesting the overwhelming stability of the C_s ($^2A'$) structure as the global minimum of $Nb_2O_5^-$.

The ground state for Nb_2O_5 neutral is C_s ($^1A'$) (Figure 3b), differing only slightly from the global minimum of the anion. A low-lying D_{3h} ($^1A_1'$) isomer is located at 0.16 eV above the ground state, which possesses three bridging O atoms (Figure 3c). Other structures are at least ∼0.9 eV higher in energy (Figure S2, Supporting Information).

4.2. $Ta_2O_5^-$ and Ta_2O_5. The potential energy surfaces for $Ta_2O_5^-$ and Ta_2O_5 are the same as those for the Nb systems. The ground state for $Ta_2O_5^-$ is C_s ($^2A'$) (Figure 3d), which is the same as that for $Nb_2O_5^-$. Similar to the Nb_2O_5 neutral, the D_{3h} ($^1A_1'$) (Figure 3e) and C_s ($^1A'$) (Figure 3f) states for Ta_2O_5 are close in energy, except that their energy order reverses: The D_{3h} ($^1A_1'$) state becomes lowest in energy for Ta_2O_5, with the C_s ($^1A'$) state being marginally higher in energy by 0.14 eV. Alternative optimized structures are at least ∼1.5 and ∼1.2 eV higher in energy for $Ta_2O_5^-$ (Figure S7, Supporting Information) and Ta_2O_5 (Figure S8, Supporting Information), respectively.

4.3. $Nb_2O_6^-$ and Nb_2O_6. The ground-state structure for $Nb_2O_6^-$ is C_s ($^2A'$) (Figure 4a), which is also based on the four-membered Nb_2O_2 ring with four terminal O atoms. The bridging Nb−O distances are slightly uneven (2.054 versus 1.889 Å). Of the four terminal Nb−O distances, three are around 1.75−1.76 Å whereas the other one is quite elongated (1.936 Å).

Table 1. Observed Adiabatic and Vertical Detachment Energies (ADEs and VDEs) from the Photoelectron Spectra, Compared to the Calculated Ground State ADEs and VDEs at the B3LYP Level of Theory

	feature	ADE (exptl)[a,b,c]	VDE (exptl)[a,b]	ADE (B3LYP)[a]	VDE (B3LYP)[a]
$Nb_2O_5^-$	X	3.33 (5)	3.58 (5)	3.42	3.79
	A		5.65 (5)		
	B		6.32 (3)		
$Nb_2O_6^-$	X	5.35 (5)	5.74 (3)	5.17	5.61
	A		6.29 (3)		
$Nb_2O_7^-$	X	5.25 (5)	5.64 (3)	5.07	5.51
	A		6.25 (3)		
$Ta_2O_5^-$	X	3.71 (5)	3.99 (5)	3.56	4.05
	A		5.55 (5)		
	B		6.31 (3)		
$Ta_2O_6^-$	X	5.28 (5)	5.57 (3)	5.08	5.43
	A		6.28 (3)		
$Ta_2O_7^-$	X	5.15 (5)	5.49 (3)	4.95	5.32
	A		6.22 (3)		

[a] All energies are in eV. [b] Numbers in parentheses represent the experimental uncertainties in the last digit. [c] Electron affinity of the neutral species.

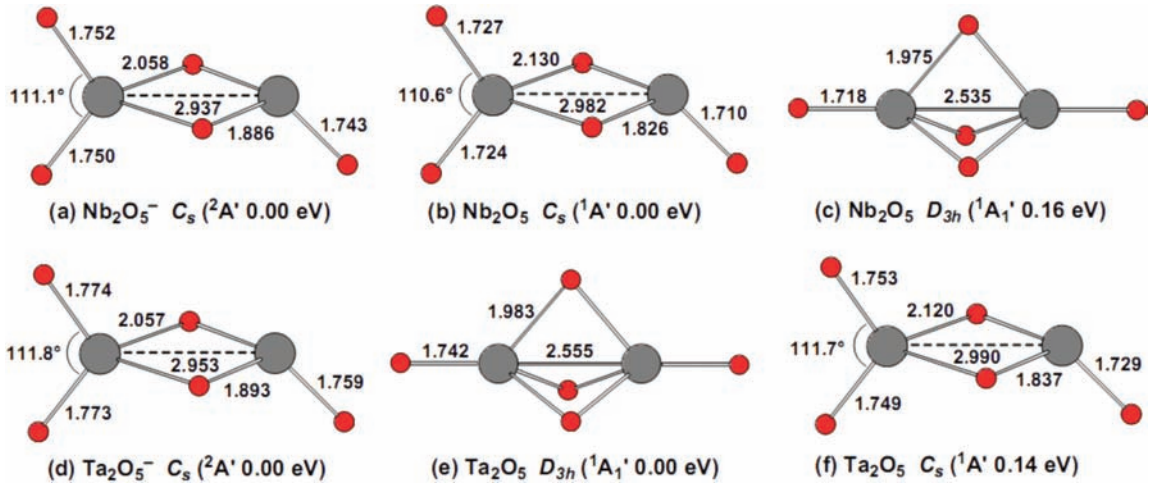

Figure 3. Optimized ground-state and low-lying structures (within ~0.5 eV) for $M_2O_5^-$ and M_2O_5 (M = Nb, Ta) at the B3LYP level. Bond distances (in Angstroms) and selected bond angles (deg) are shown.

A low-lying C_s ($^2A''$) state is located 0.27 eV higher in energy (Figure 4b), which is similar to the ground state in terms of atomic connectivity and characteristic bond distances. The corresponding quartet and sextet states are 3.12 and 6.78 eV above the ground state, respectively (Figure S3, Supporting Information). Other four-membered Nb_2O_2 ring-based structures, with three terminal O atoms on the same Nb center or with a terminal O_2 unit, are at least 2.4 eV higher than the ground state. Alternative optimized structures with one bridging oxygen, three bridging oxygens, or no bridging oxygen are also higher in energy (by 2.7−9.6 eV; Figure S3, Supporting Information).

A similar set of structures is optimized for the Nb_2O_6 neutral (Figure S4, Supporting Information). The C_{2h} (^3B_u) (Figure 4c) and C_{2v} ($^3B_2$) (Figure 4d) structures are found to be virtually degenerate (within 0.02 eV), both of which are triplet states. These structures each feature two elongated Nb−O terminal bonds (~1.9 Å), differing only in their trans versus cis arrangements. The closest singlet structure, C_{2v} ($^1A_1$), is 0.15 eV higher in energy (Figure 4e), with four bridging oxygens including a substantially elongated O_2 unit (1.457 Å). Alternative optimized neutral structures are at least 0.7 eV above the ground state (Figure S4, Supporting Information).

4.4. $Nb_2O_7^-$ and Nb_2O_7. The ground state of $Nb_2O_7^-$ is C_s ($^2A''$) (Figure 4f), which can be viewed as built from the C_s ($^2A'$) ground-state structure of $Nb_2O_6^-$ by replacing the elongated terminal oxygen with an O_2 unit. Alternative optimized anion structures are at least 1 eV higher in energy (Figure S5, Supporting Information). The neutral ground state, C_s ($^3A''$) (Figure 4g), shows similar structural characteristics relative to its anion, except that one terminal Nb−O distance is elongated (1.907 Å). A similar C_s ($^3A'$) state is located 0.35 eV above the neutral ground state (Figure 4h), whereas alternative neutral structures are much higher in energy (>0.8 eV; Figure S6, Supporting Information).

4.5. $Ta_2O_n^-$ and Ta_2O_n (n = 6, 7). The potential energy surfaces of $Ta_2O_n^-$ and Ta_2O_n (n = 6, 7) (Figures S9−S12, Supporting Information) are similar to those of the $Nb_2O_n^-$ and Nb_2O_n counterparts. The calculated ground-state and low-lying

dx.doi.org/10.1021/ja110061v | J. Am. Chem. Soc. 2011, 133, 3085–3094

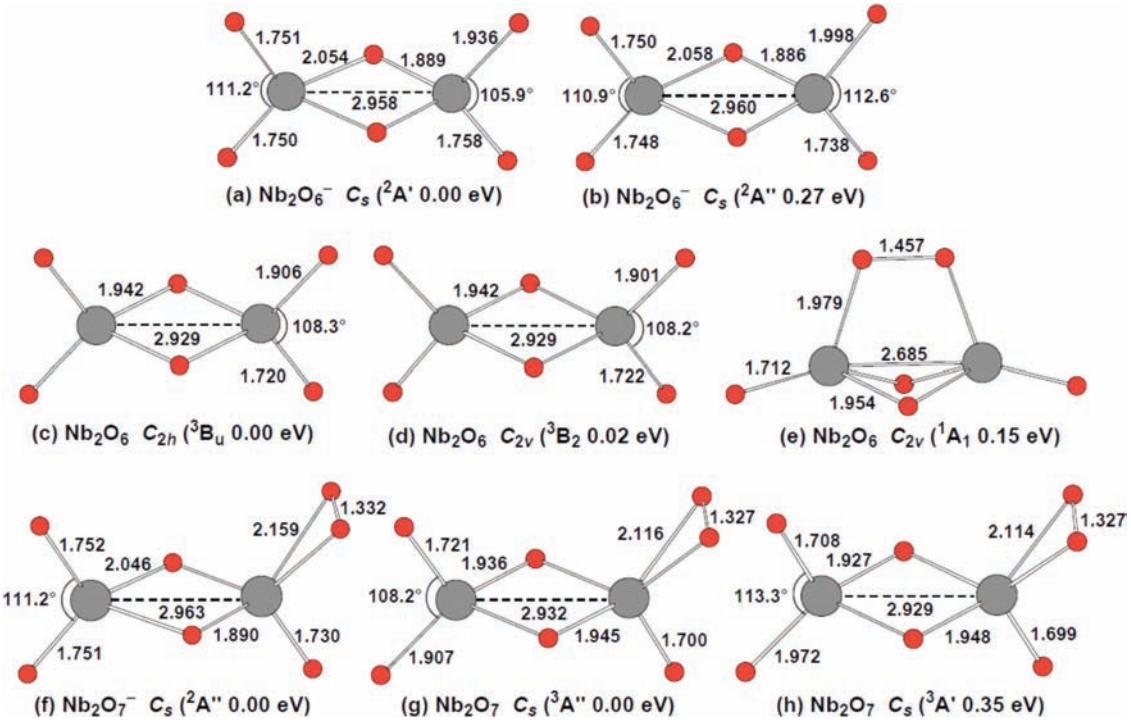

Figure 4. Optimized ground-state and low-lying structures (within ~0.5 eV) for $Nb_2O_n^-$ and Nb_2O_n (n = 6, 7) at the B3LYP level. Bond distances (in Angstroms) and selected bond angles (deg) are shown.

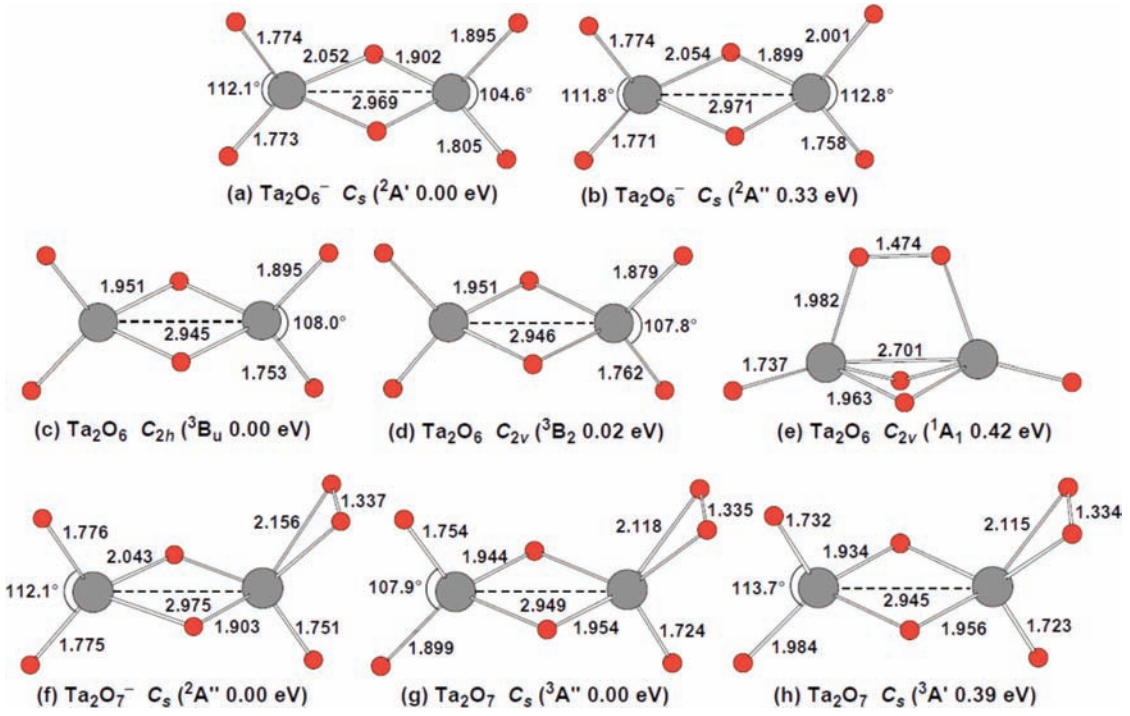

Figure 5. Optimized ground-state and low-lying structures (within ~0.5 eV) for $Ta_2O_n^-$ and Ta_2O_n (n = 6, 7) at the B3LYP level. Bond distances (in Angstroms) and selected bond angles (deg) are shown.

structures for $Ta_2O_n^-$ and Ta_2O_n (n = 6, 7) are summarized in Figure 5, which show one-to-one correspondence to those of $Nb_2O_n^-$ and Nb_2O_n (Figure 4), except for very minor changes in bond angles and bond distances. It is noted that while the majority of terminal and bridging M−O bonds in the ground-state structures show slight expansions from Nb to Ta, the elongated M−O bonds undergo slight contractions and the O−O distances in the O_2 units show slight expansions, hinting that the Ta centers can probably stabilize the unusual oxygen species and activate O_2 better.

dx.doi.org/10.1021/ja110061v |*J. Am. Chem. Soc.* 2011, 133, 3085–3094

Table 2. Relative Energies of the Low-Lying States of the $M_2O_n^-$ (M = Nb, Ta; n = 5−7) Clusters at the B3LYP Level (within ~0.5 eV), and Comparisons with Those from the CCSD(T) Single-Point Calculations at the B3LYP Geometries

	electronic state	B3LYP[a,b]	CCSD(T)[a,c]
Nb_2O_5	C_s (^{1}A′)	0.00	0.00
	D_{3h} (^{1}A$_1$′)	0.16	0.14
Ta_2O_5	D_{3h} (^{1}A$_1$′)	0.00	0.00
	C_s (^{1}A′)	0.14	0.28
$Nb_2O_6^-$	C_s (^{2}A′)	0.00	0.00
	C_s (^{2}A″)	0.27	0.24
$Ta_2O_6^-$	C_s (^{2}A′)	0.00	0.00
	C_s (^{2}A″)	0.33	0.24
Nb_2O_6	C_{2h} (^{3}B$_u$)	0.00	0.17
	C_{2v} (^{3}B$_2$)	0.02	0.20
	C_{2v} (^{1}A$_1$)	0.15	0.00
Ta_2O_6	C_{2h} (^{3}B$_u$)	0.00	0.00
	C_{2v} (^{3}B$_2$)	0.02	0.06
	C_{2v} (^{1}A$_1$)	0.42	0.02
Nb_2O_7	C_s (^{3}A″)	0.00	0.00
	C_s (^{3}A′)	0.35	0.32
Ta_2O_7	C_s (^{3}A″)	0.00	0.00
	C_s (^{3}A′)	0.39	0.34

[a] All energies are in eV. [b] Optimized at the B3LYP/Nb,Ta/Stuttgart+2f1g/O/aug-cc-pVTZ level. [c] Single-point energy at the CCSD(T)/Nb,Ta/Stuttgart+2f1g/O/aug-cc-pVTZ//B3LYP/Nb,Ta/Stuttgart+2f1g/O/aug-cc-pVTZ level.

4.6. CCSD(T) Single-Point Calculations for Low-Lying Cluster Structures. The relative energies for the low-lying $M_2O_n^-$ and M_2O_n (M = Nb, Ta; n = 5−7) cluster structures (within ~0.5 eV at B3LYP level; Figures 3−5) were further calculated using single-point CCSD(T) calculations at the B3LYP geometries. The results are summarized in Table 2. It can be seen that the energetics from the CCSD(T) calculations are in line with the B3LYP results except for the ground state of Nb_2O_6. Further theoretical calculations with more sophisticated methods, such as full CCSD(T) structural optimization, may be necessary to resolve the true ground state of Nb_2O_6, but these are computationally not feasible for us currently. It should be stressed that the current experiment starts with the $Nb_2O_6^-$ C_s (^{2}A′) cluster anion and, upon photodetachment, only probes the C_{2h} (^{3}B$_u$) and C_{2v} (^{3}B$_2$) final states of the Nb_2O_6 neutral cluster. We will not be able to access the Nb_2O_6 C_{2v} (^{1}A$_1$) state even if it is indeed slightly lower in energy. Thus, we believe the B3LYP results are generally solid for our discussion below.

5. COMPARISON BETWEEN EXPERIMENT AND THEORY

5.1. $Nb_2O_5^-$ and $Ta_2O_5^-$. The C_s (^{2}A′) structures (Figure 3a and 3d) are clearly the ground states for $Nb_2O_5^-$ and $Ta_2O_5^-$, with alternative structures (Figures S1 and S7, Supporting Information) being at least ~1.2 and ~1.5 eV higher in energy, respectively. The calculated ground-state VDEs at the B3LYP level are 3.79 eV for $Nb_2O_5^-$ and 4.05 eV for $Ta_2O_5^-$ (Table 1), which are compared to the experimental values of 3.58 and 3.99 eV, respectively. The B3LYP method appears to slightly overestimate the binding energies with an error of 0.21 and 0.06 eV, respectively. The simulated PES spectra for $Nb_2O_5^-$ (Figure 6a) and $Ta_2O_5^-$ (Figure 6d) agree well with the experimental data, reproducing the characteristic X−A energy gaps and the overall patterns.

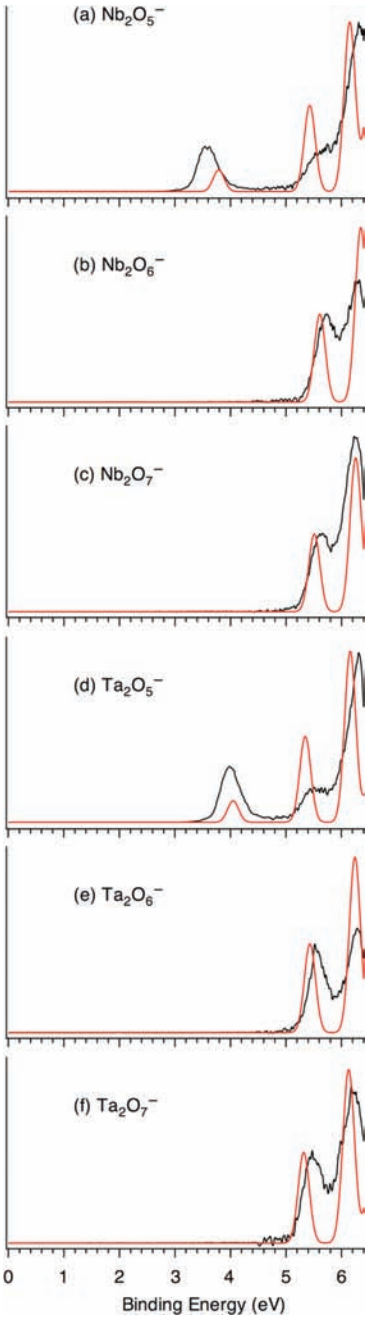

Figure 6. Simulated photoelectron spectra (red curves) for $Nb_2O_n^-$ and $Ta_2O_n^-$ (n = 5−7) based on their ground-state structures, compared to experimental spectra (black curves). The simulations are done by fitting the distribution of calculated vertical detachment energies with unit-area Gaussian functions of 0.1 eV width.

5.2. $Nb_2O_n^-$ and $Ta_2O_n^-$ (n = 6, 7). All $M_2O_n^-$ and M_2O_n (M = Nb, Ta; n = 6, 7) clusters are O-rich species, consistent with the observed high electron affinities for the neutrals: 5.35, 5.25, 5.28, and 5.15 eV for Nb_2O_6, Nb_2O_7, Ta_2O_6, and Ta_2O_7, respectively (Table 1), which are among the highest in gas-phase molecules,[50] suggesting that these neutral clusters are extremely

strong oxidizers. The ground-state VDEs for $Nb_2O_6^-$, $Nb_2O_7^-$, $Ta_2O_6^-$, and $Ta_2O_7^-$ are measured to be 5.74, 5.64, 5.57, and 5.49 eV, respectively. For comparison, the calculated VDEs at the B3LYP level for the anion ground-state structures are 5.61, 5.51, 5.43, and 5.32 eV along the same series, which nicely correlate with the experimental trend. The computational data consistently underestimates the experimental values by marginal errors (0.13−0.17 eV). The simulated PES spectra for the four clusters agree well with the experimental data (Figure 6). We found that band A involves multiple electronic transitions with close binding energies (see Table S1 in the Supporting Information), and the average of the calculated VDEs agrees perfectly with the experimental measurements (errors = 0.01−0.09 eV). The frontier MOs for all four anions consist primarily of O 2p atomic orbitals from the terminal O atoms (M═O), consistent with their similar experimental PES patterns. Overall, the agreement between experimental and theory is excellent, lending considerable credence to the identified anion ground-state structures and the suitability of the B3LYP method.

6. DISCUSSION

6.1. Radicals, Diradicals, and Superoxides in $M_2O_n^-$ and M_2O_n (M = Nb, Ta; n = 6, 7). The ground-state structures for the O-rich $M_2O_n^-$ and M_2O_n (M = Nb, Ta; n = 6, 7) clusters are similar in terms of atomic connectivity, symmetry and electronic state, and bond distances (Figures 4 and 5), consistent with their similar PES patterns (Figures 1 and 2). An examination of the bond distances between Nb (Ta) and O shows the following. (i) The bridging bond distances average at ∼1.96 Å for both Nb and Ta, and typical terminal M−O bonds average at ∼1.74 Å for Nb and ∼1.76 Å for Ta, which can be roughly attributed to M−O single bonds and M═O double bonds, respectively. (ii) The elongated M−O terminal bonds average at ∼1.92 Å for Nb and ∼1.90 Å for Ta, which are substantially longer than the M═O double bonds and may be assigned as $M-O^\bullet$ single bonds, that is, single bonds between Nb (Ta) centers and oxygen radicals ($O^\bullet$). (iii) The distances between Nb (Ta) centers and the terminal O_2 units average at ∼2.14 Å for both Nb and Ta. These are assigned as the $M-(O_2^\bullet)$ bonds involving a superoxide ($O_2^\bullet$) unit, in which the bond order between the Nb (Ta) center and the O atom may be formally considered as 0.5. (iv) The O−O bond order in the superoxide units is 1.5, whose calculated distances average at ∼1.33 Å for Nb and ∼1.34 Å for Ta, in line with the gas-phase value for superoxide (1.341 Å).[3] Following these bond order assignments, the chemical bonding in the clusters can be understood on the basis of Lewis structures.

The structures of all eight O-rich anion and neutral clusters are based on the M_2O_2 four-membered ring motif, in which each Nb (Ta) center is tetracoordinated with two bridging O units and two terminal O or O_2 units (Figures 4 and 5). In their favorite +5 formal oxidation states, tetracoordination is not optimal for the Nb (Ta) centers if only terminal M═O double bonds and bridging M−O single bonds are involved, providing the primary electronic driving force for oxygen activation in Nb/Ta oxide clusters. We performed electron density analyses to shed further light on the nature of the radical, diradical, and superoxide species. The four oxygen-rich anion clusters (Figure 7, left column) each possess an unpaired spin, primarily localized on a terminal O atom in $Nb_2O_6^-$ and $Ta_2O_6^-$ and equally shared by the two O atoms in the O_2 unit in $Nb_2O_7^-$ and $Ta_2O_7^-$, resulting in radical ($O^{-\bullet}$) and superoxide ($O_2^{-\bullet}$) species, respectively.

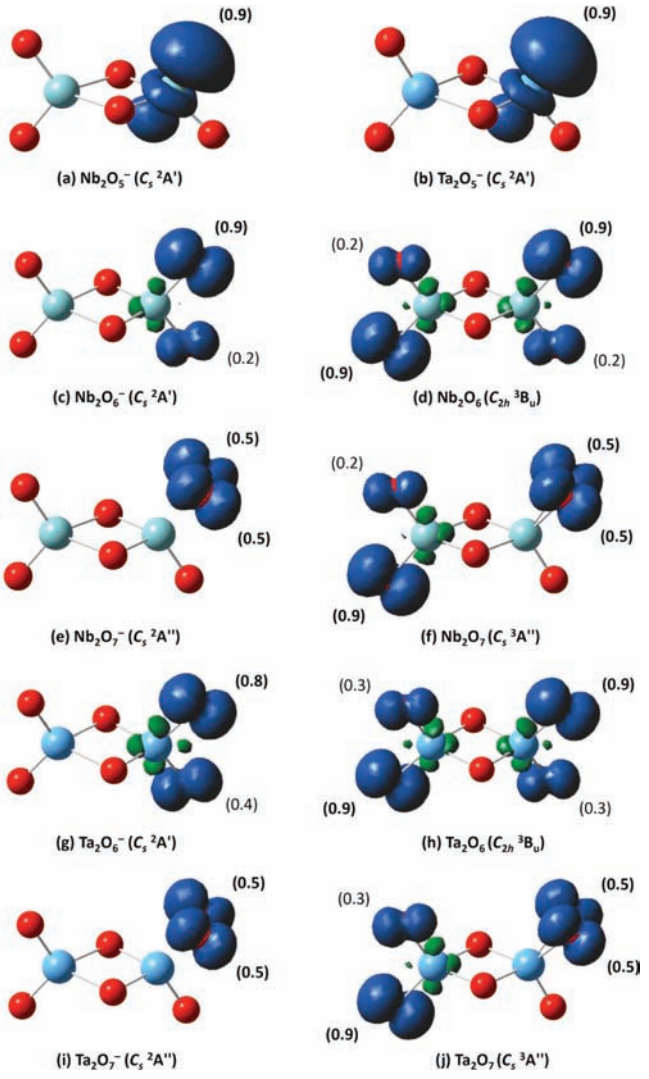

Figure 7. Numerical electron spin density (in |e|) for the ground states of $M_2O_n^-$ (n = 5−7) and M_2O_n (n = 6, 7) clusters. All other O atoms have a spin density of 0.0 (not labeled).

The four oxygen-rich neutral clusters (Figure 7, right column) each possess two unpaired spins, which form diradical species ($O^\bullet + O^\bullet$) in Nb_2O_6 and Ta_2O_6 and ($O^\bullet + O_2^\bullet$) in Nb_2O_7 and Ta_2O_7. Note that due to relativistic effects in the 5d element,[51] there is a slight increase of d electron in the spin density from Nb to Ta. Oxygen radicals and superoxides have been widely discussed in the oxide surface chemistry[3] and in transition-metal oxide clusters.[10−15,25,26] Such species are expected to be highly reactive toward H abstraction or other oxidation reactions and may play significant roles in the surface chemistry of Nb and Ta oxides. However, report of these transient species on Nb and Ta oxide surfaces has been elusive. In gas-phase clusters, an IR-MPI study assigned a superoxide ($O_2^\bullet$) unit in the cationic $Nb_2O_6^+$ cluster,[10] whereas a combined IR-MPI and DFT study by Sauer and co-workers,[14] with the aid of experimental PES data,[52] revealed superoxides in valent isoelectronic $V_2O_7^-$ and V_2O_7 clusters.

Other types of active oxygen species can also be found in the Nb (Ta) oxide clusters. For example, the low-lying isomeric C_{2v} ($^1A_1$) states of Nb_2O_6 and Ta_2O_6 (Figures 4e and 5e) possess a

dx.doi.org/10.1021/ja110061v |J. Am. Chem. Soc. 2011, 133, 3085–3094

highly activated O_2 unit (O−O bond distances = 1.457−1.474 Å) in a bridging fashion, which is peroxide in nature (O_2^{2-} = 1.49 Å)[3] and may be viewed as the fusion of two $O^•$ radicals. These structures can be constructed from the C_{2v} ($^3B_2$) structures (Figures 4d and 5d) by bending two terminal $O^•$ radicals toward each other and pairing up the two unpaired spins, at the expense of a small overall energy penalty (0.1−0.4 eV). In fact, the C_{2v} ($^1A_1$) structures can be described as classical Lewis structures, in which each Nb (Ta) center forms three M−O single bonds and one M═O double bond and the peroxide unit possesses an O−O single bond. These classical M_2O_6 C_{2v} ($^1A_1$) structures, along with the classical M_2O_5 D_{3h} ($^1A_1'$) structures (Figure 3c and 3e), help define the "ideal" bridging M−O and terminal M═O bond distances in the gas phase, which average at 1.97, 1.98, 1.72, 1.74 Å for Nb−O, Ta−O, Nb═O, and Ta═O bonds, respectively. A direct implication from these values is that those bridging M−O and terminal M═O bonds in the ground-state structures of $M_2O_n^-$ and M_2O_n (M = Nb, Ta, n = 5−7; Figures 3−5) deviate somewhat from the ideal single and double bonds, as anticipated.

6.2. $M_2O_7^-$ and M_2O_7 as Molecular Models for Dioxygen Activation by $M_2O_5^{-/0}$: $M_2O_5^{-/0} + O_2 \rightarrow M_2O_7^{-/0}$. The observations of superoxide species in $M_2O_7^-$ and M_2O_7 provide us with an excellent opportunity to study the activation of O_2 by the $M_2O_5^-$ and M_2O_5 clusters, which is of fundamental interest in the surface chemistry of Nb and Ta oxides.[5−9] The $M_2O_7^{-/0}$ clusters may be formed by $M_2O_5^{-/0} + O_2$, as schematically illustrated in Figure 8. The energetics of the O_2 addition reactions are evaluated at the B3LYP level:

$$Nb_2O_5^-(C_s, {}^2A') + O_2 \rightarrow Nb_2O_7^-(C_s, {}^2A'') - 3.00\ \text{eV} \quad (1)$$

$$Nb_2O_5(C_s, {}^1A') + O_2 \rightarrow Nb_2O_7(C_s, {}^3A'') - 1.34\ \text{eV} \quad (2)$$

$$Ta_2O_5^-(C_s, {}^2A') + O_2 \rightarrow Ta_2O_7^-(C_s, {}^2A'') - 3.14\ \text{eV} \quad (3)$$

$$Ta_2O_5(C_s, {}^1A') + O_2 \rightarrow Ta_2O_7(C_s, {}^3A'') - 1.90\ \text{eV} \quad (4)$$

The $M_2O_5^-$ anions are shown to have a localized spin on the tricoordinate metal site, which is effectively a reduced M^{4+} defect site (Figure 7a and 7b). An O_2 molecule readily chemisorbs at the M^{4+} site via charge transfer (Figure 8a), giving rise to a superoxide ($O_2^{-•}$) species with a substantial chemisorption energy (3.00 eV for M = Nb; 3.14 eV for M = Ta). Consequently, the dioxygen is activated as shown from the elongated O−O distances: 1.332−1.337 Å in $O_2^{-•}$ (Figures 4f and 5f) versus 1.21 Å in free O_2.[3]

The O_2 adsorption energies on neutral M_2O_5 clusters are calculated to be 1.34 eV for M = Nb and 1.90 eV for M = Ta. These large adsorption energies are surprising, considering the fact that M_2O_5 are closed-shell stoichiometric clusters and are expected to be relatively inert. The large adsorption energies are due to the formation of triplet M_2O_7 products, which are essentially diradicals. Thus, the M_2O_5 reactions with O_2 to form M_2O_7 can be viewed to involve promotion of an electron from O 2p to the metal d orbitals, as schematically shown in Figure 8b. This promotion would induce a large energy barrier for the O_2 adsorption process. This energy barrier is the HOMO−LUMO gap, as measured from the PES spectra (Figures 1a and 2a), ∼1.8 and ∼1.4 eV for Nb_2O_5 and Ta_2O_5, respectively. Even though this is a substantial barrier, it is much lower compared to those in the bulk oxides (3.4 eV for Nb_2O_5; 3.5−4.5 eV for Ta_2O_5)[53,54] or the corresponding tetrahedral cage M_4O_{10} clusters (3.88 eV for Nb_4O_{10}; 3.87 eV for Ta_4O_{10}).[27] In photocatalysis, for example, such barriers for the neutral M_2O_5 clusters are relatively small and can be easily overcome by visible or near-infrared photons.

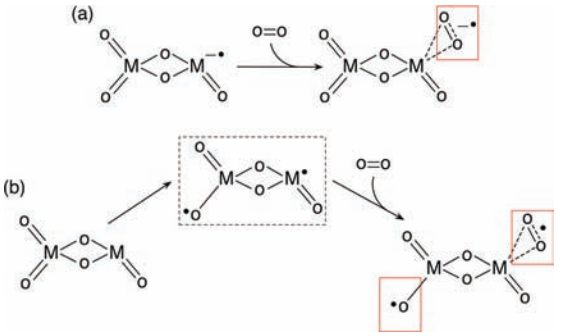

Figure 8. Schematic of the (a) O_2 adsorption on C_s ($^2A'$) $M_2O_5^-$ (M = Nb, Ta) anions via charge transfer, generating C_s ($^2A''$) $M_2O_7^-$ with a superoxide ($O_2^{-•}$) unit, and (b) O_2 adsorption on C_s ($^1A'$) M_2O_5 (M = Nb, Ta) neutrals via a proposed intermediate triplet state, resulting in C_s ($^3A''$) M_2O_7 with radical ($O^•$) and superoxide ($O_2^•$) units.

Thus, the M_2O_5 (M = Nb, Ta) clusters are very different from the stoichiometric W_2O_6 cluster, which only forms a van der Waals complex with O_2 in W_2O_8 via physisorption (<0.1 eV),[26] even though $W_2O_8^-$ contains a superoxide analogous to that in $M_2O_7^-$ (M = Nb, Ta). Note that, however, the strengths for typical M═O double bonds are comparable for the three elements: 7.53, 8.70, and 7.46 eV for Nb═O, Ta═O, and W═O, respectively.[55] The O_2 chemisorption energies on the 3d counterparts, $V_2O_5^-$ and V_2O_5, are calculated (at the same level) to be 1.89 and 0.92 eV, respectively, which are markedly lower than those for Nb (Ta) oxides but differ qualitatively from those for W oxides.[56] Therefore, the Nb and Ta oxide clusters appear to possess superior abilities to activate O_2, due in part to the existence of tricoordinate Nb (Ta) sites, which facilitate stronger interactions with O_2. The current results may shed light on the surface chemistry of Nb (Ta) oxides, such as their remarkable properties as catalytic promoters, which are poorly understood at the molecular level.[5−9]

6.3. Benchmarks of DFT Methods. One of the values of cluster studies is to provide quantitative data to verify theoretical methods.[57,58] The current PES data yield relatively accurate electron binding energies for the Nb and Ta oxide clusters (Table 1), which can be utilized to benchmark the performance of various density functionals. The experimental ground-state VDEs for the four oxygen-rich $M_2O_n^-$ (M = Nb, Ta; n = 6, 7) clusters are compared with the DFT results at the B3LYP, BP86, and PW91 levels (Figure 9). The BP86 and PW91 functionals are shown to severely underestimate the binding energies and fail to reproduce the trend of the binding energies. In particular, the BP86 functional fails severely in the case of $Ta_2O_7^-$ (by 0.40 eV), whereas PW91 fails for both $Nb_2O_7^-$ and $Ta_2O_7^-$ (by 0.49 and 0.46 eV, respectively). It seems that the superoxide species in $Nb_2O_7^-$ and $Ta_2O_7^-$ pose greater challenges for pure DFT methods such as BP86 and PW91, likely associated with their deficiency in describing the O−O bonding.[2] On the other hand, the hybrid B3LYP functional works well for all species, faithfully reproducing the experimental binding energy trend along the series with a consistent, small error (0.13−0.17 eV). Thus, the B3LYP method performs better for Nb and Ta oxide clusters,

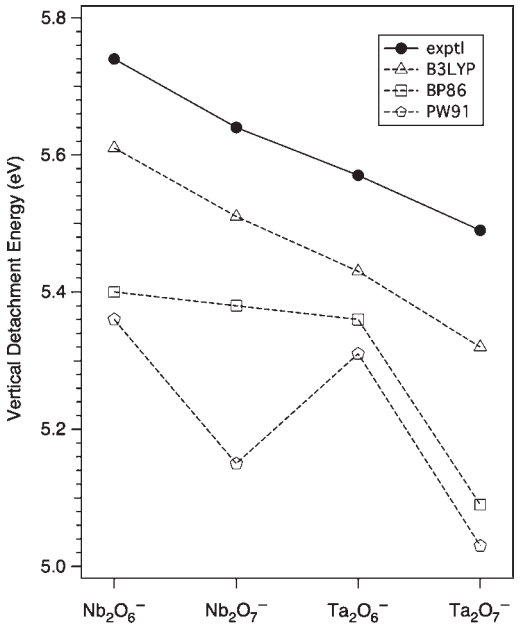

Figure 9. Comparison of the experimental ground-state vertical detachment energies (solid dots) for oxygen-rich $M_2O_n^-$ (M = Nb, Ta; n = 6, 7) clusters with those calculated using the B3LYP (empty triangles), BP86 (empty squares), and PW91 (empty pentagons) methods.

both qualitatively and quantitatively. This information should be valuable for computational modeling of the bulk and surface properties of Nb/Ta oxides.

7. CONCLUSIONS

We studied the electronic structure of stoichiometric and O-rich Nb and Ta oxide clusters, $M_2O_n^-$ and M_2O_n (M = Nb, Ta; n = 5−7), via anion photoelectron spectroscopy and density-functional calculations. Large HOMO−LUMO gaps are observed for the stoichiometric clusters, whereas very high electron binding energies are measured for the O-rich clusters (>5.1 eV). Structural searches at the B3LYP level show that all the O-rich clusters are open-shell: doublets for the anions and triplets for the neutrals. Spin density analyses reveal oxygen radical, diradical, and superoxide characters for the O-rich anion and neutral species. The $M_2O_7^-$ and M_2O_7 clusters both contain an activated O_2 unit and can be viewed as formed by O_2 chemisorption to the stoichiometric clusters, $M_2O_5^-$ and M_2O_5, respectively. The O_2 adsorption on $M_2O_5^-$ yields $M_2O_7^-$ with a superoxide unit (via charge transfer). The adsorption energies on the stoichiometric M_2O_5 neutrals are surprisingly high (1.3−1.9 eV), yielding the M_2O_7 diradicals, which also contain an activated O_2. The current results suggest that structural defects in Nb and Ta oxides should possess superior properties for O_2 activation. The experimental data have also been used to benchmark the performance of B3LYP, BP86, and PW91 functionals, and B3LYP is found to perform much better for Nb and Ta oxide systems.

■ ASSOCIATED CONTENT

Ⓢ Supporting Information. Observed vertical detachment energies for $Nb_2O_n^-$ and $Ta_2O_n^-$ (n = 5−7) clusters and their comparison with those calculated at the B3LYP level (Table S1), alternative optimized anion and neutral cluster structures at the B3LYP level (Figures S1−S12) and their Cartesian coordinates (Tables S2 and S3), and complete ref 48. This material is available free of charge via the Internet at http://pubs.acs.org.

■ AUTHOR INFORMATION

Corresponding Author
xhuang@fzu.edu.cn; Lai-Sheng_Wang@brown.edu

■ ACKNOWLEDGMENT

This work was supported by the Chemical Sciences, Geosciences and Biosciences Division, Office of Basic Energy Sciences, U.S. Department of Energy (DOE) under grant no. DE-FG02-03ER15481 (catalysis center program). X.H. gratefully acknowledges supports from the Natural Science Foundation of China (20771026, 21071031, and 90922022) and the Natural Science Foundation of Fujian Province of China (no. 2008J0151).

■ REFERENCES

(1) (a) Henrich, V. E.; Cox, P. A. *The Surface Science of Metal Oxides*; Cambridge University Press: Cambridge, 1994. (b) Freund, H.-J.; Kuhlenbeck, H.; Staemmler, V. *Rep. Prog. Phys.* **1996**, *59*, 283. (c) Freund, H.-J.; Pacchioni, G. *Chem. Soc. Rev.* **2008**, *37*, 2224.

(2) Ganduglia-Pirovano, M. V.; Hofmann, A.; Sauer, J. *Surf. Sci. Rep.* **2007**, *62*, 219.

(3) For reviews on mononuclear and molecular oxygen species on metal oxide surfaces, see:(a) Che, M.; Tench, A. J. *Adv. Catal.* **1982**, *31*, 77. (b) Che, M.; Tench, A. J. *Adv. Catal.* **1983**, *32*, 1. (c) Anpo, M.; Che, M.; Fubini, B.; Garrone, E.; Giamello, E.; Paganini, M. C. *Top. Catal.* **1999**, *8*, 189.

(4) (a) Wachs, I. E.; Weckhuysen, B. M. *Appl. Catal., A* **1997**, *157*, 67. (b) Weckhuysen, B. M.; Keller, D. E. *Catal. Today* **2003**, *78*, 25.

(5) (a) Tanabe, K.; Okazaki, S. *Appl. Catal., A* **1995**, *133*, 191. (b) Tanabe, K. *Catal. Today* **2003**, *78*, 65.

(6) Ziolek, M. *Catal. Today* **2003**, *78*, 47.

(7) Ushikubo, T. *Catal. Today* **2000**, *57*, 331.

(8) Guerrero-Perez, M. O.; Banares, M. A. *Catal. Today* **2009**, *142*, 245.

(9) Kudo, A.; Miseki, Y. *Chem. Soc. Rev.* **2009**, *38*, 253.

(10) Fielicke, A.; Meijer, G.; von Helden, G. *J. Am. Chem. Soc.* **2003**, *125*, 3659.

(11) (a) Justes, D. R.; Mitric, R.; Moore, N. A.; Bonacic-Koutecky, V.; Castleman, A. W., Jr. *J. Am. Chem. Soc.* **2003**, *125*, 6289. (b) Johnson, G. E.; Mitric, R.; Tyo, E. C.; Bonacic-Koutecky, V.; Castleman, A. W., Jr. *J. Am. Chem. Soc.* **2008**, *130*, 13912. (c) Johnson, G. E.; Tyo, E. C.; Castleman, A. W., Jr. *Proc. Natl. Acad. Sci. U.S.A.* **2008**, *105*, 18108. (d) Johnson, G. E.; Mitric, R.; Nossler, M.; Tyo, E. C.; Bonacic-Koutecky, V.; Castleman, A. W., Jr. *J. Am. Chem. Soc.* **2009**, *131*, 5460. (e) Nossler, M.; Mitric, R.; Bonacic-Koutecky, V.; Johnson, G. E.; Tyo, E. C.; Castleman, A. W., Jr. *Angew. Chem., Int. Ed.* **2010**, *49*, 407.

(12) (a) Dong, F.; Heinbuch, S.; Xie, Y.; Rocca, J. J.; Bernstein, E. R.; Wang, Z. C.; Deng, K.; He, S. G. *J. Am. Chem. Soc.* **2008**, *130*, 1932. (b) Zhao, Y. X.; Wu, X. N.; Wang, Z. C.; He, S. G.; Ding, X. L. *Chem. Commun.* **2010**, *46*, 1736. (c) Ma, J. B.; Wu, X. N.; Zhao, Y. X.; Ding, X. L.; He, S. G. *J. Phys. Chem. A* **2010**, *114*, 10024.

(13) (a) Feyel, S.; Döbler, J.; Schröder, D.; Sauer, J.; Schwarz, H. *Angew. Chem., Int. Ed.* **2006**, *45*, 4681. (b) Schröder, D.; Schwarz, H. *Proc. Natl. Acad. Sci. U.S.A.* **2008**, *105*, 18114.

(14) Santambrogio, G.; Brümmer, M.; Wöste, L.; Döbler, J.; Sierka, M.; Sauer, J.; Meijer, G.; Asmis, K. R. *Phys. Chem. Chem. Phys.* **2008**, *10*, 3992.

(15) Zhao, Y. Y.; Zheng, X. M.; Zhou, M. F. *Chem. Phys.* **2008**, *351*, 13.

(16) (a) Sigsworth, S. W.; Castleman, A. W., Jr. *J. Am. Chem. Soc.* **1992**, *114*, 10471. (b) Deng, H. T.; Kerns, K. P.; Castleman, A. W., Jr. *J. Phys. Chem.* **1996**, *100*, 13386. (c) Zemski, K. A.; Bell, R. C.;

Castleman, A. W., Jr. *J. Phys. Chem. A* **2000**, *104*, 5732. (d) Zemski, K. A.; Justes, D. R.; Bell, R. C.; Castleman, A. W., Jr. *J. Phys. Chem. A* **2001**, *105*, 4410. (e) Zemski, K. A.; Justes, D. R.; Castleman, A. W., Jr. *J. Phys. Chem. A* **2001**, *105*, 10237. (f) Justes, D. R.; Moore, N. A.; Castleman, A. W., Jr. *J. Phys. Chem. B* **2004**, *108*, 3855.

(17) (a) Jackson, P.; Fisher, K. J.; Willett, G. D. *Int. J. Mass Spectrom.* **2000**, *197*, 95. (b) Jackson, P.; Fisher, K. J.; Willett, G. D. *Chem. Phys.* **2000**, *262*, 179.

(18) Fielicke, A.; Meijer, G.; von Helden, G. *Eur. Phys. J. D* **2003**, *24*, 69.

(19) Molek, K. S.; Jaeger, T. D.; Duncan, M. A. *J. Chem. Phys.* **2005**, *123*, 144313.

(20) Dong, F.; Heinbuch, S.; He, S. G.; Xie, Y.; Rocca, J. J.; Bernstein, E. R. *J. Chem. Phys.* **2006**, *125*, 164318.

(21) (a) Asmis, K. R.; Santambrogio, G.; Brümmer, M.; Sauer, J. *Angew. Chem., Int. Ed.* **2005**, *44*, 3122. (b) Janssens, E.; Santambrogio, G.; Brümmer, M.; Wöste, L.; Lievens, P.; Sauer, J.; Meijer, G.; Asmis, K. R. *Phys. Rev. Lett.* **2006**, *96*, 233401. (c) Li, S.; Mirabal, A.; Demuth, J.; Wöste, L.; Siebert, T. *J. Am. Chem. Soc.* **2008**, *130*, 16832.

(22) Fialko, E. F.; Kikhtenko, A. V.; Goncharov, V. B.; Zamaraev, K. I. *J. Phys. Chem. B* **1997**, *101*, 5772.

(23) Waters, T.; O'Hair, R. A. J.; Wedd, A. G. *J. Am. Chem. Soc.* **2003**, *125*, 3384.

(24) (a) Wyrwas, R. B.; Yoder, B. L.; Maze, J. T.; Jarrold, C. C. *J. Phys. Chem. A* **2006**, *110*, 2157. (b) Mayhall, N. J.; Rothgeb, D. W.; Hossain, E.; Raghavachari, K.; Jarrold, C. C. *J. Chem. Phys.* **2009**, *130*, 124313.

(25) Zhai, H. J.; Kiran, B.; Cui, L. F.; Li, X.; Dixon, D. A.; Wang, L. S. *J. Am. Chem. Soc.* **2004**, *126*, 16134.

(26) Huang, X.; Zhai, H. J.; Waters, T.; Li, J.; Wang, L. S. *Angew. Chem., Int. Ed.* **2006**, *45*, 657.

(27) Zhai, H. J.; Döbler, J.; Sauer, J.; Wang, L. S. *J. Am. Chem. Soc.* **2007**, *129*, 13270.

(28) Zhai, H. J.; Averkiev, B. B.; Zubarev, D. Yu.; Wang, L. S.; Boldyrev, A. I. *Angew. Chem., Int. Ed.* **2007**, *46*, 4277.

(29) (a) Huang, X.; Zhai, H. J.; Kiran, B.; Wang, L. S. *Angew. Chem., Int. Ed.* **2005**, *44*, 7251. (b) Zhai, H. J.; Wang, L. S. *J. Am. Chem. Soc.* **2007**, *129*, 3022. (c) Zhai, H. J.; Li, S. G.; Dixon, D. A.; Wang, L. S. *J. Am. Chem. Soc.* **2008**, *130*, 5167. (d) Zubarev, D. Yu.; Averkiev, B. B.; Zhai, H. J.; Wang, L. S.; Boldyrev, A. I. *Phys. Chem. Chem. Phys.* **2008**, *10*, 257. (e) Zhai, H. J.; Wang, L. S. *Chem. Phys. Lett.* **2010**, *500*, 185.

(30) (a) Zhai, H. J.; Wang, B.; Huang, X.; Wang, L. S. *J. Phys. Chem. A* **2009**, *113*, 3866. (b) Zhai, H. J.; Wang, B.; Huang, X.; Wang, L. S. *J. Phys. Chem. A* **2009**, *113*, 9804. (c) Chen, W. J.; Zhai, H. J.; Zhang, Y. F.; Huang, X.; Wang, L. S. *J. Phys. Chem. A* **2010**, *114*, 5958.

(31) Böhme, D. K.; Schwarz, H. *Angew. Chem., Int. Ed.* **2005**, *44*, 2336.

(32) Song, L.; Eychmuller, A.; St. Pierre, R. J.; El-Sayed, M. A. *J. Phys. Chem.* **1989**, *93*, 2485.

(33) (a) Athanassenas, K.; Kreisle, D.; Collings, B. A.; Rayner, D. M.; Hackett, P. A. *Chem. Phys. Lett.* **1993**, *213*, 105. (b) Yang, D. S.; Zgierski, M. Z.; Rayner, D. M.; Hackett, P. A.; Martinez, A.; Salahub, D. R.; Roy, P. N.; Carrington, T., Jr. *J. Chem. Phys.* **1995**, *103*, 5335.

(34) (a) Green, S. M. E.; Alex, S.; Fleischer, N. L.; Millam, E. L.; Marcy, T. P.; Leopold, D. G. *J. Chem. Phys.* **2001**, *114*, 2653. (b) Zheng, W. J.; Li, X.; Eustis, S.; Bowen, K. *Chem. Phys. Lett.* **2008**, *460*, 68.

(35) (a) Sambrano, J. R.; Andres, J.; Beltran, A.; Sensato, F.; Longo, E. *Chem. Phys. Lett.* **1998**, *287*, 620. (b) Martinez, A.; Calaminici, P.; Koster, A. M.; Salahub, D. R. *J. Chem. Phys.* **2001**, *114*, 819. (c) Calaminici, P.; Flores-Moreno, R.; Koster, A. M. *J. Chem. Phys.* **2004**, *121*, 3558. (d) Wu, Z. J.; Kawazoe, Y.; Meng, J. *J. Mol. Struct. (THEOCHEM)* **2006**, *764*, 123.

(36) (a) Wang, L. S.; Cheng, H. S.; Fan, J. *J. Chem. Phys.* **1995**, *102*, 9480.(b) Wang, L. S.; Wu, H. In *Advances in Metal and Semiconductor Clusters*; Duncan, M. A., Ed.; JAI Press: Greenwich, CT, 1998; Vol. 4, Cluster Materials, pp 299−343.

(37) (a) Wang, L. S.; Li, X. In *Cluster and Nanostructure Interfaces*; Jena, P., Khanna, S. N., Rao, B. K., Eds.; World Scientific: River Edge, NJ, 2000; pp 293−300. (b) Akola, J.; Manninen, M.; Hakkinen, H.; Landman, U.; Li, X.; Wang, L. S. *Phys. Rev. B* **1999**, *60*, R11297. (c) Wang, L. S.; Li, X.; Zhang, H. F. *Chem. Phys.* **2000**, *262*, 53. (d) Zhai, H. J.; Wang, L. S.; Alexandrova, A. N.; Boldyrev, A. I. *J. Chem. Phys.* **2002**, *117*, 7917.

(38) (a) Becke, A. D. *J. Chem. Phys.* **1993**, *98*, 1372. (b) Lee, C.; Yang, W.; Parr, R. G. *Phys. Rev. B* **1988**, *37*, 785.

(39) Stephens, P. J.; Devlin, F. J.; Chabalowski, C. F.; Frisch, M. J. *J. Phys. Chem.* **1994**, *98*, 11623.

(40) Andrae, D.; Haeussermann, U.; Dolg, M.; Stoll, H.; Preuss, H. *Theor. Chim. Acta* **1990**, *77*, 123.

(41) Küchle, W.; Dolg, M.; Stoll, H.; Preuss, H. Pseudopotentials of the Stuttgart/Dresden Group 1998, revision August 11, 1998; http://www.theochem.uni-stuttgart.de/pseudopotentiale.

(42) Martin, J. M. L.; Sundermann, A. *J. Chem. Phys.* **2001**, *114*, 3408.

(43) (a) Dunning, T. H., Jr. *J. Chem. Phys.* **1989**, *90*, 1007. (b) Kendall, R. A.; Dunning, T. H., Jr.; Harrison, R. J. *J. Chem. Phys.* **1992**, *96*, 6796.

(44) Tozer, D. J.; Handy, N. C. *J. Chem. Phys.* **1998**, *109*, 10180.

(45) (a) Purvis, G. D., III; Bartlett, R. J. *J. Chem. Phys.* **1982**, *76*, 1910. (b) Scuseria, G. E.; Janssen, C. L.; Schaefer, H. F., III. *J. Chem. Phys.* **1988**, *89*, 7382. (c) Raghavachari, K.; Trucks, G. W.; Pople, J. A.; Head-Gordon, M. *Chem. Phys. Lett.* **1989**, *157*, 479. (d) Watts, J. D.; Gauss, J.; Bartlett, R. J. *J. Chem. Phys.* **1993**, *98*, 8718. (e) Bartlett, R. J.; Musial, M. *Rev. Mod. Phys.* **2007**, *79*, 291.

(46) (a) Becke, A. D. *Phys. Rev. A* **1988**, *38*, 3098. (b) Perdew, J. P. *Phys. Rev. B* **1986**, *33*, 8822.

(47) (a) Burke, K.; Perdew, J. P.; Wang, Y. In *Electronic Density Functional Theory: Recent Progress and New Directions*; Dobson, J. F., Vignale, G., Das, M. P., Eds.; Plenum: New York, 1998. (b) Perdew, J. P.; Wang, Y. *Phys. Rev. B* **1992**, *45*, 13244.

(48) Frisch, M. J.; et al. *Gaussian 03*, revision D.01; Gaussian, Inc.: Wallingford, CT, 2004.

(49) Werner, H.-J.; Knowles, P. J.; Lindh, R.; Manby, F. R.; Schütz, M.; et al. *MOLPRO*, version 2010.1, a package of ab initio programs; See http://www.molpro.net.

(50) (a) Rienstra-Kiracofe, J. C.; Tschumper, G. S.; Schaefer., H. F.; Nandi, S.; Ellison, G. B. *Chem. Rev.* **2002**, *102*, 231. (b) Gutsev, G. L.; Boldyrev, A. I. *Adv. Chem. Phys.* **1985**, *61*, 169.

(51) Pyykkö, P. *Chem. Rev.* **1988**, *88*, 563.

(52) Zhai, H. J.; Wang, L. S. *J. Chem. Phys.* **2002**, *117*, 7882.

(53) (a) Duffy, M. T.; Wang, C. C.; Waxman, A.; Zaininger, K. H. *J. Electrochem. Soc.* **1969**, *116*, 234. (b) Yoshimura, K.; Miki, T.; Iwama, S.; Tanemura, S. *Thin Solid Films* **1996**, *281*, 235.

(54) (a) Khawaja, E. E.; Tomlin, S. G. *Thin Solid Films* **1975**, *30*, 361. (b) Tepehan, F. Z.; Ghodsi, F. E.; Ozer, N.; Tepehan, G. G. *Sol. Energy Mater. Sol. Cells* **1997**, *46*, 311. (c) Ghodsi, F. E.; Tepehan, F. Z. *Sol. Energy Mater. Sol. Cells* **1999**, *59*, 367. (d) Afanas'ev, V. V.; Stesmans, A.; Zhao, C.; Caymax, M.; Rittersma, Z. M.; Maes, J. W. *Appl. Phys. Lett.* **2005**, *86*, 072108.

(55) Luo, Y. R. In *CRC Handbook of Chemistry and Physics*, 91st ed; Haynes, W. M., Ed.; CRC Press: Boca Raton, FL, 2010.

(56) The O_2 adsorption energies on stoichiometric V, Nb, Ta, and W oxide clusters decrease along $Ta_2O_5 \rightarrow Nb_2O_5 \rightarrow V_2O_5 \rightarrow W_2O_6$, with a chemisorption-to-physisorption transition from V_2O_5 (0.92 eV) to W_2O_6 (<0.1 eV). For the stoichiometric anion clusters, the O_2 adsorption energies also decrease along $Ta_2O_5^- \rightarrow Nb_2O_5^- \rightarrow V_2O_5^- \rightarrow W_2O_6^-$ but an abrupt change takes place from $Nb_2O_5^-$ (3.00 eV) to $V_2O_5^-$ (1.89 eV). This combination shows that the Nb (Ta) oxide clusters clearly have the advantages in O_2 chemisorption, because both their anionic and neutral clusters can interact strongly with O_2, correlating well with the unique catalytic properties of Nb (Ta) oxides.[5−9]

(57) (a) Li, S. G.; Dixon, D. A. *J. Phys. Chem. A* **2006**, *110*, 6231. (b) Li, S. G.; Dixon, D. A. *J. Phys. Chem. A* **2007**, *111*, 11093. (c) Li, S. G.; Dixon, D. A. *J. Phys. Chem. A* **2007**, *111*, 11908. (d) Li, S. G.; Dixon, D. A. *J. Phys. Chem. A* **2008**, *112*, 6646. (e) Li, S. G.; Zhai, H. J.; Wang, L. S.; Dixon, D. A. *J. Phys. Chem. A* **2009**, *113*, 11273.

(58) Cramer, C. J.; Truhlar, D. G. *Phys. Chem. Chem. Phys.* **2009**, *11*, 10757.